NUMERICAL COMPUTATIONS OF STORM SURGES WITHOUT BOTTOM STRESS

CHESTER P. JELESNIANSKI

Environmental Science Services Administration, Washington, D.C.

ABSTRACT

A numerical storm surge model, using the linearized form of the transport equations, is used to compute surges in a rectangular basin of variable depth and with three open water boundaries. The computed surges are sensitive to the initial placements of model tropical storms that are stationary, very slow moving, or moving parallel to the coast at any speed. These storms generate shelf seiches and a type of resurgent edge wave of significant amplitude. On the other hand, the computed surges are almost insensitive to initial placement of moderate and fast-moving storms.

The numerical model is used to construct a prototype prediction system in the form of polar graphs which give coastal surge magnitude and dispersion against storm strength and speed and direction of motion.

LIST OF SYMBOLS

D	depth of undisturbed fluid
p	atmospheric surface pressure
$(p_\infty - p_0)$	pressure drop of model storm from center of storm to large distance
R	radius of model storm's maximum wind
U	transport in x-direction
U_s	uniform linear speed or motion of storm
V	transport in y-direction
v	wind speed at any surface point (anemometer level) of model stationary storm
V_R	maximum wind of stationary model storm
V_s	wind speed of moving model storm
f	Coriolis parameter
g	gravity
h	disturbance in the height of free surface
k_s	tangential friction coefficient of model storm
k_n	normal friction coefficient of model storm
r	distance from storm center
Φ	direction of storm motion (mathematical sense: angles are measured counterclockwise from the x-coordinate axis)
θ	polar angle (storm center at origin)
ϕ	inflow or ingress angle (angle of wind across isobars) of stationary storm
ρ	density of basin fluid
ρ_a	air density
τ	wind stress vector on basin's fluid
β	angle between sloping bottom of a basin and the horizontal
γ	latitude
λ	wavelength
κ	wave number

1. INTRODUCTION

Past solutions for the storm surge or meteorological tide problem were obtained by analytical and empirical methods. These gave valuable insight into the problem but they have serious restrictions. The analytical methods (Kajiura [9]) deal only with very simple models because of the complex nature and mathematical intractability of the general storm surge equations of motion, while the empirical methods (Harris [5]) suffer from a paucity of actual observed storms and lack of data.

It now appears that the best hope for further insight into the problem will come from numerical computations. Initial studies in this direction have been made by Hansen [4], who dealt with the action of an idealized driving force in the North Sea, and Platzman [15], who dealt with an idealized pressure jump crossing an enclosed lake.

Recently, Ueno [20] and Miyazaki [12] dealt with empirical driving forces from observed tropical storms traveling in an ocean, and computed the coastal surges by numerical means. These studies were intended to be as complete as possible and considered non-linear bottom friction, map scale factors, variations of the Coriolis parameter, etc. There was good agreement between observed and computed surges.

The purpose of the present paper is not to expand on the above studies, but to describe an experiment with a simpler model developed by Harris and Jelesnianski [7] and Jelesnianski [8], using idealized storms and basins with a restricted number of physical parameters. From computational experiments, involving variation of these parameters, much insight can be gained as to the relative significance of the various physical processes involved.

The parameters used consist of the Coriolis parameter (assumed constant), basin depth profile (one-dimensional), stationary storm maximum wind, radius of maximum wind, and uniform rectilinear storm velocity.

The numerical computations utilize the linearized form of the transport equations of motion without bottom friction. Bottom friction is one of the least understood phenomena and its introduction has been deliberately delayed while gaining other useful knowledge of storm-induced tides. For storms traveling at moderate or high speed with limited time on the continental shelf, the

effect of bottom friction on the coastal surge is small (Kajiura [9]). It was empirically determined by test computations that the coastal surge is insensitive to any bottom friction law, including a no-friction law, during landfall of moderate and fast-moving storms. For slow or stagnating storms, the surge to the right of landfall (observer on sea, facing land) is relatively insensitive to the friction law used, except for damping of shelf seiches, whereas to the left of landfall the surge profile has wide variations.

For storms located near and traveling parallel to the coast in a basin of sloping depth, the numerical model has some deficiencies without bottom friction. Under these conditions, the model generates resurgences or edge waves (Greenspan [3], Lamb [10], Reid [16], Ursell [21]). These resurgences, forming behind the storm's track as distinguished from the immediately formed and directly generated surge, have differing amplitudes and periods according to the friction law used.

The present numerical model is most suitable for model storms of small areal extent, moving rapidly, and crossing the coast at or near normal incidence. In this study the storms generally have a speed ≥ 10 m.p.h. and cross the coastline at an acute angle of at least 30°. The initial position of the storm's center is placed at least beyond the continental shelf. To test the surge model, comparisons are made between computed and observed surges for hurricanes Audrey (1957) and Carla (1961) that affected the Gulf States.

The results of this series of experiments provide further insight into the storm surge problem, point out areas for future research, and at the same time present some operational techniques for forecasting storm surges generated by tropical storms.

2. STORM SURGE MODEL

The storm surge model consists of a model storm traveling across a rectangular shaped basin of variable depth and with three open boundaries. In the numerical program the storm and fluid in the basin are initially quiescent; the driving forces are allowed to grow to maturity in a continuous manner (Jelesnianski [8]). A linearized form of the transport equations without bottom friction (Harris and Jelesnianski [7]) was used:

$$\left.\begin{aligned}\frac{\partial U}{\partial t}&=-gD(x,y)\frac{\partial h}{\partial x}+fV+\frac{D(x,y)}{\rho}\frac{\partial p}{\partial x}+{}^{(x)}\tau(x,y,t)/\rho\\ \frac{\partial V}{\partial t}&=-gD(x,y)\frac{\partial h}{\partial y}-fU+\frac{D(x,y)}{\rho}\frac{\partial p}{\partial y}+{}^{(y)}\tau(x,y,t)/\rho\\ \frac{\partial h}{\partial t}&=-\frac{\partial U}{\partial x}-\frac{\partial V}{\partial y}\end{aligned}\right\}\cdot \quad (1)$$

A list of symbols is given at the beginning of this article. Gravity g, has the value 32.2 ft./sec.^{2} The Coriolis parameter f is constant (generally for latitude 30°), thereby excluding planetary waves. The equations consider barotropic, inertio-gravitational waves.

The driving forces due to pressure and wind are determined from model tropical storms (see Appendix 1). The surface stress components, ${}^{(x)}\tau$, ${}^{(y)}\tau$ are assumed to be a quadratic function of the wind speed,

$$\frac{{}^{(x)}\tau}{\rho}=\frac{k\rho_a}{\rho}|\mathbf{V}_s|{}^{(x)}V_s;\ \frac{{}^{(y)}\tau}{\rho}=\frac{k\rho_a}{\rho}|\mathbf{V}_s|{}^{(y)}V_s \quad (2)$$

where ρ_a, the density of air (1.15×10^{-3} gm./cm.^{3}), is constant, and ${}^{(x)}V_s$, ${}^{(y)}V_s$ are surface wind components. The non-dimensional value used for $k\rho_a/\rho$ is 3×10^{-6}. Although equation (2) is not universally accepted, it is used as a convenience and compromise between many formulations (Wilson [22]). The units chosen for the transport equations give h, the surge, in feet.

Figure 1 illustrates the type of basin used in this study. It has three open boundaries; the boundary conditions are: no transport normal to the closed coast, static heights on the deep water open boundary (zero heights in the absence of the pressure driving force), and vanishing normal derivatives of transport on the two remaining open boundaries. The one-dimension depth profile is a convenient idealization of the Atlantic and Gulf coasts of the United States.

Figure 2 illustrates an idealization of the depth profile normal to a natural coast.[1] The "berm" and "dune" are the first and last line of natural defense against the onslaught of battering surface waves and storm surges. The numerical model is not strongly dependent on the actual choice of boundary depth, even if it be zero, since this term enters only as a factor of the pressure gradient which in shallow water is about two orders of magnitude less than the wind stress (Jelesnianski [8]). This weak dependence was borne out through trial computations; accordingly the linear extrapolation of the bottom profile to point O′ in figure 2 was used to represent the depth at the coast. Only if the depths away from the boundary, especially at points A and B, are varied is there significant variation of surge values. The inserted vertical wall is a convenience to simulate the rapidly changing depths at a coastal region. This system allows negative surges on the boundary, avoids the problem of moving boundaries, and gives a finite ratio of surge to depth on the boundary providing the surge does not touch bottom.

The numerical forms used for equation (1) are those given by Harris and Jelesnianski [7] and Jelesnianski [8]. Grid distances were generally 4 mi., except for some specialized computations in which a distance of 2 mi. was used along the coastal region. The time intervals between computations were generally 2.5 min.

For purposes of convenience in later sections, we now define a *standard storm* as one with maximum (stationary storm) wind of 100 m.p.h. and located at latitude 30°; a *standard basin* is one having the depth profile of figure 1. Unless stated to the contrary, the observer will always be located at sea and facing the coastal boundary.

[1] See any "Coast and Harbor Chart," U.S. Coast and Geodetic Survey.

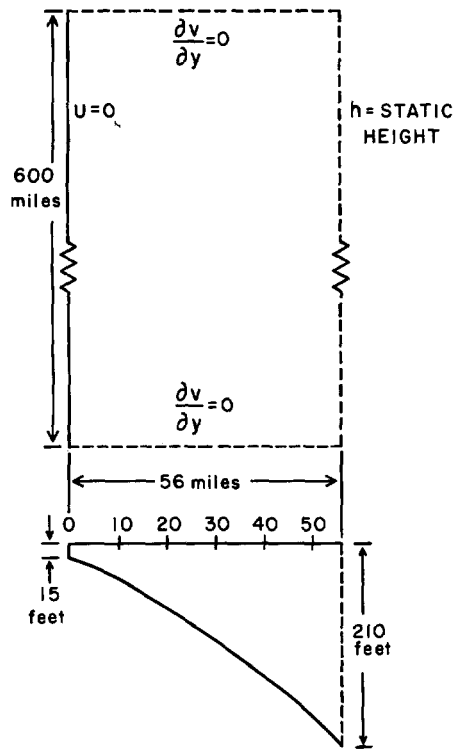

FIGURE 1.—Plan and vertical section views of the standard model basin used in this study.

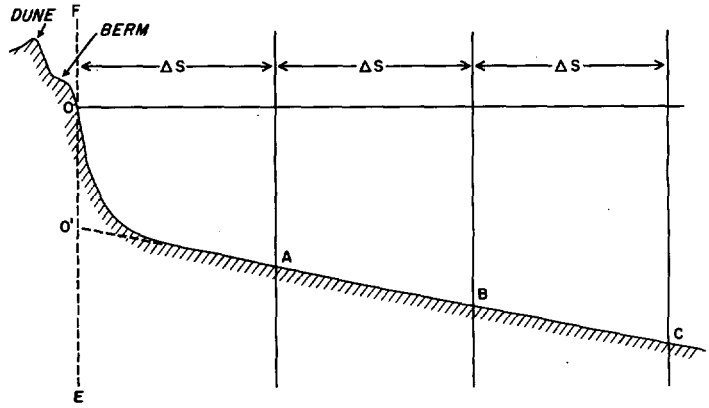

FIGURE 2.—An idealization of the depth profile about a coastal region. Δs is the grid distance used in the numerical model. The vertical wall EF simulates the rapidly changing depths of the immediate coastal region.

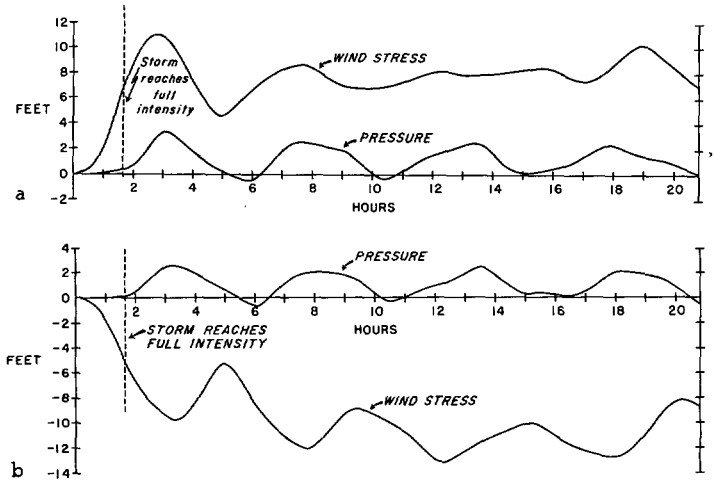

FIGURE 3.—Oscillations of the storm surge with time on points of the coastline for the separate driving forces of pressure and wind. The storm is stationary with center on the coast. (a) 32 mi. to the right of the storm center; observer on sea facing land. (b) 40 mi. to the left of the storm center.

3. APPLICABILITY OF THE MODEL WITHOUT BOTTOM STRESS

The numerical model without bottom stress cannot handle all conceivable situations and must be restricted to prescribed ranges of storm speed, and direction of storm motion in the basin. These ranges were subjectively determined by trial experiments through comparison of the surge profiles with and without bottom friction. If the differences in the compared surge profiles were small, then the movement vector of the storm was considered applicable.

Results of trial experiments appear to give reasonable surges for storms moving moderately or very fast along paths that cross the coast at an angle not too small. For other vector storm motions, the model generates shelf seiches and resurgences of large amplitude or large transport values along the coast; these features are objectionable and should be excluded from the model. For very slowly moving storms, the model generates shelf seiches of significent amplitude. For storms of large areal extent, enormous transports eventually form in the coastal regions. This situation can be controlled with the introduction of bottom friction, but there is great variance in the damping effects on the seiches with different dissipating mechanisms.

With or without bottom friction (neglecting seiches, and storms of large areal extent), the most significant difference in the coastal surge profile exists to the left of landfall. For an example of this situation, consider a standard storm, with radius of maximum winds equal to 30 mi., remaining stationary with its center on the midpoint of a standard basin's coastal segment. The computed surge from this storm showed oscillations with time at each point of the coast. In figure 3 are shown the oscillations, for the wind and pressure driving forces separately, for two points on the coast located 32 mi. to the right and 40 mi. to the left of the storm's center. The amplitudes and periods do not systematically change with time, suggesting that the oscillations are not the result of impulsive generation. Plots made of the surge profile on the coast at discrete time intervals demonstrated that the water level oscillated up and down as a shelf seiche (see Appendix 2). The same computations were performed

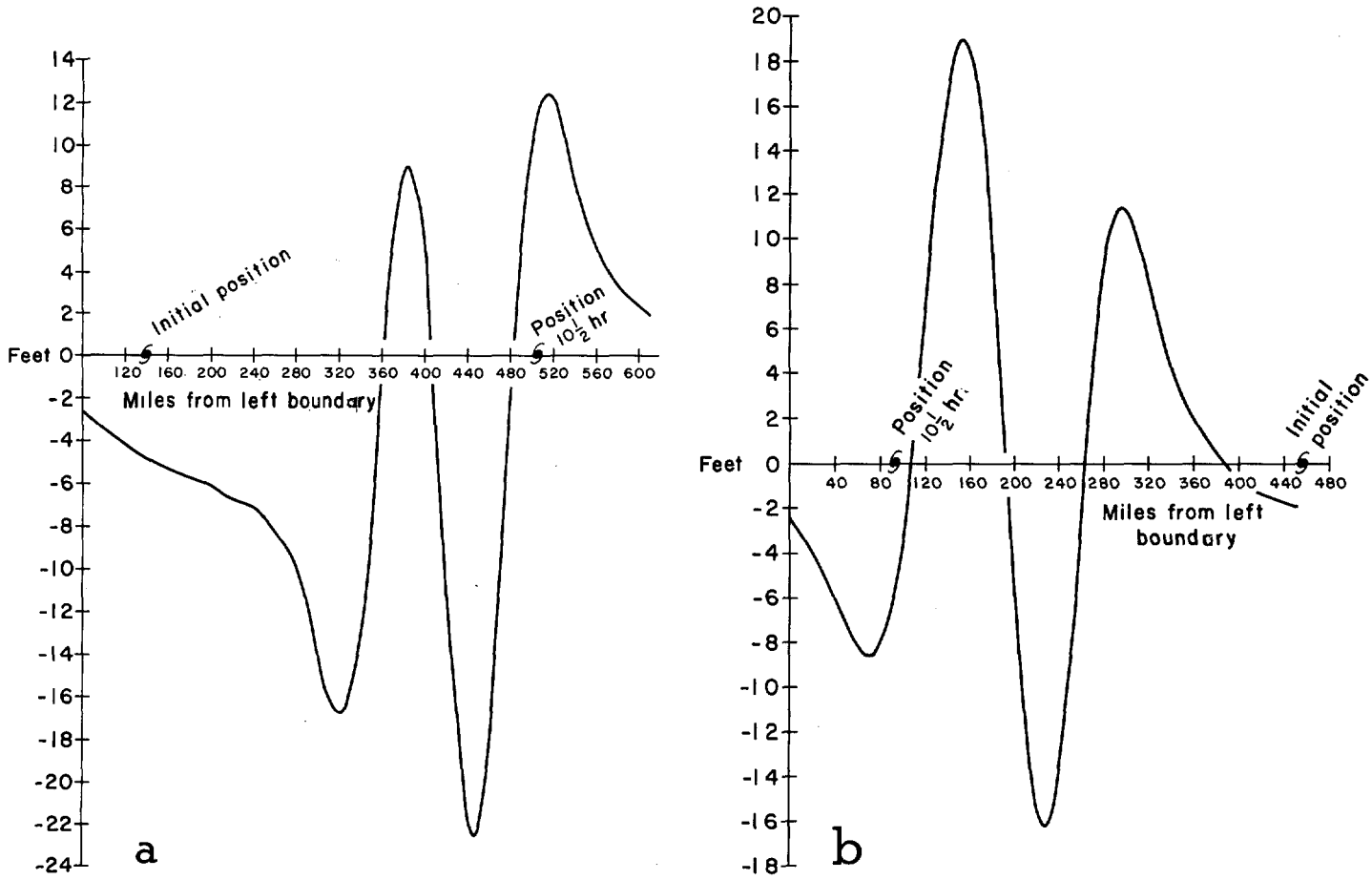

FIGURE 4.—Storm surge on the coast 10½ hr. after initialization. The abscissa is the coastline. The observer is on sea facing land. The storm travels parallel to the coast at 35 m.p.h. The driving forces are superimposed. (a) Storm moving to the right. (b) Storm moving to the left.

with grid distances of 2 mi. in the region near the coast and the storm's radius of maximum winds halved to 15 mi. The periods did not differ significantly from those of figure 3. This also suggests that the oscillations are mainly a shelf seiche.

Therefore in this study, for storms of large areal extent, we will consider only those that travel at speeds $\geq$ 10 m.p.h., for, in this case, the seiches are not unreasonably large and there are not large differences in the computations with or without bottom stress.

Another situation that generates large amplitudes in the numerical model without bottom friction occurs when a storm travels parallel or nearly parallel to the coast with its center in shallow water. Figure 4 shows plots of the water level on the coast 10½ hr. after initialization of computations for the storm considered above with its center now moving along the coast, both to right and left, at 35 m.p.h. In both cases there was a train of waves of rather large amplitude behind, but not in front of, the storm's track on the coast. When moved to the right the storm generated a large negative surge, whereas when moved to the left it generated a large positive surge.

It has been suggested that the resurgences behind the storm's track could be edge waves (Reid [16]). These waves, if excited, occur in a semi-infinite uniform sloping depth basin having a straight coastline. The basin (fig. 1) used in the present computations does not exactly fit this geometry (because of the vertical wall and non-constant slope), but as a first approximation it is assumed that the basin can generate a wave which closely approaches the edge wave phenomenon.

The rear portion of the resurgent wave trains should travel along the coast with group velocity (Munk [13]). Reid [16] gives the group velocity of edge waves traveling in either direction on the coast as $(g \sin \beta) \cdot (4g\kappa \sin \beta + f^2)^{-1/2}$. Because program limitations permitted only a relatively short time span for the model storm moving parallel to the model coast, the numerically computed speed for the rear of the wave train could not be exactly determined; qualitatively, it appears to be of the order given by Reid [16]. Separate calculations were made for storms traveling parallel to the coast with differing constant speeds; the computed resurgence amplitudes were larger for storms traveling with greater speed.

It is interesting to view the surge with time at a fixed point on the coast. Figure 5 shows such oscillations, as

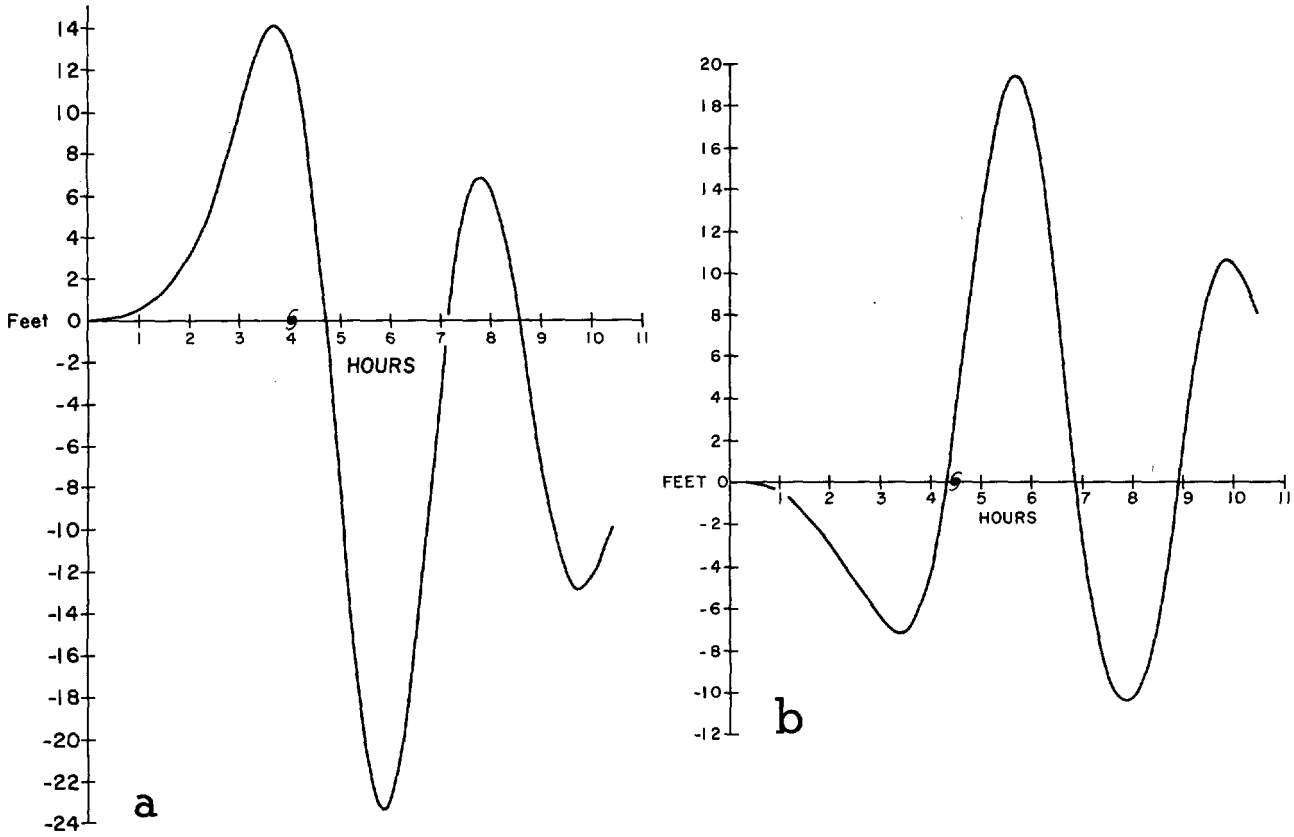

FIGURE 5.—The surge height at a fixed point on the coast with time for passage of a storm moving parallel to the coast at 35 m.p.h. (a) Storm moving to the right. (b) Storm moving to the left.

would be observed by tide gages, for the traveling storms. Figures 4 and 5 show that the oscillations or resurgences are traveling waves and not seiches.

The directly generated surge (i.e., the first peak to the right of the storm center) should not be confused with the resurgences. If the last crest and trough of the wave train behind the storm's track in figure 4 are considered to be part of the resurgence, then the resurgent wavelengths are almost the same in both figures, about 135 mi.

Reid [16] gives the edge wave frequency (fundamental mode) as,

$$\omega=-\frac{f}{2}\mp\sqrt{g\kappa\sin\beta+\left(\frac{f}{2}\right)^2}. \tag{3}$$

The wave number κ is positive. The two frequencies are for waves moving on the coast to the right and left respectively. If the phase velocity of the resurgent waves were equal to the longshore storm velocity, then by (3),

$$\lambda=\frac{2\pi|\mathbf{U}_s|^2}{g\sin\beta-f|\mathbf{U}_s|}.$$

In this case the wavelength does not depend on direction of storm movement along the coast. If $\sin\beta=200$ ft./56 mi. for the model basin and $f=0.73\times10^{-4}$/sec., then for $|\mathbf{U}_s|=35$ m.p.h., the wavelength becomes 144 mi. and agrees fairly well with the resurgences of figure 4. Separate computer runs for slower and faster moving storms showed that the wavelengths of the resurgences varied approximately as the square of the storm speed.

The amplitudes of the directly generated surge and resurgences, for storms traveling parallel to the coast, became smaller the farther the storm center was placed from the coast. Separate tests made with bottom stress served to damp the resurgences, and the damping quality depended on the type of dissipating mechanism chosen. Because of this, the treatment of resurgences has been deliberately avoided at this time and will be treated in a future paper. Hereafter we shall consider only storms that cross the coast at an acute angle of at least 30°; under these conditions any resurgences that form are of small amplitude, and bottom friction plays only a small role in the coastal surge.

4. SEPARATE EFFECTS OF THE DRIVING FORCES OF A MOVING STORM

The computed storm surge is determined by driving forces consisting of wind stress and pressure gradient. It is desirable to determine the relative effects of these two forces and to see whether the pressure driving force acts in a static sense. To do this we consider a standard storm

(radius of maximum winds 15 mi.; not of large areal extent) traveling in a standard basin. The static height of this storm is 1.85 ft. Two cases are considered: storms traveling at normal incidence to the coast but at different speeds, and storms traveling at a constant 30 m.p.h. but at different crossing angles to the coast. All storms are placed initially so that landfall occurs at the same time, except for slowly moving storms.

Figure 6 gives the numerically computed maximum storm surge height on the coast plotted against storm speed for the separate driving forces, as well as the maximum height from a superposition of these driving functions. The maximum surge associated with the pressure driving force shows more variation with storm (travel) speed than does that associated with wind stress. Notice that the resultant peak storm surge from superposition of the driving functions is not a simple addition of the two peak surges; this is so because the two coastal surge profiles are not geographically similar. For the model storm and basin considered, the greatest coastal surge maximum occurred for a storm speed of about 37 m.p.h.

Let the observer be oriented on a straight-line coast so that water is to his right and land to his left; let the direction he faces be relative north with his back to relative south along the coast. Angular crossings of the storm at the coast will now be defined in the meteorological sense; thus, a storm moving to relative north along the coast has an angular crossing from the south or 180°, one moving from sea to land and crossing the coast at normal incidence has an angular crossing from the east or 90°, one moving to relative south along the coast has an angular crossing from the north or 0°, etc.

Figure 7 illustrates the numerically computed maximum storm surge on the coast for different angular storm crossing for the separate driving forces, for a superposition of these forces, and for the absolute value of the lowest surge on the coast at time of maximum surge (the minimum surge does not necessarily occur at time of maximum surge). The maximum peak surge from superposition of forces occurred for an angular crossing of about 65°; the greater variation of this peak surge compared to those of the separate forces is due to the geographical dissimilarity of the separate coastal storm surge profiles.

Figures 6 and 7 show that the pressure driving force has important and significant dynamic effects for a moving storm and cannot be considered merely in a static sense. Henceforth, all computations will be made with a superposition of the two driving forces.

5. PROTOTYPE STORM SURGE PREDICTION SCHEME

A storm surge prediction scheme based on the numerical model and not requiring access to a computer will now be described. Pre-computed coastal surge profiles will be considered for the conditions of a standard storm traveling across a standard basin and several other variable parameters will be incorporated. Suitable modifications to the profile can then be made to accommodate storms and

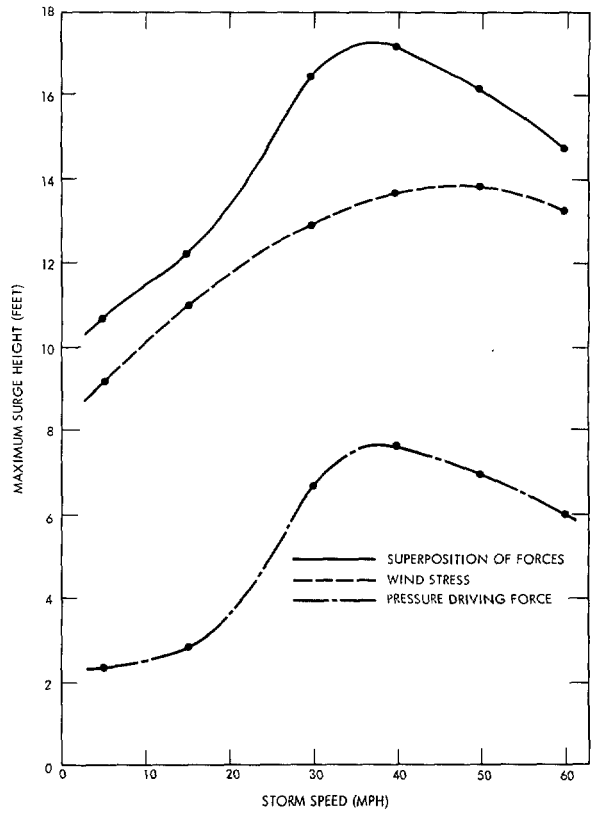

FIGURE 6.—The maximum coastal surge for the driving forces at different storm speeds; the storm's direction of motion is at normal incidence to the coast. The large dots are values for actual computer runs.

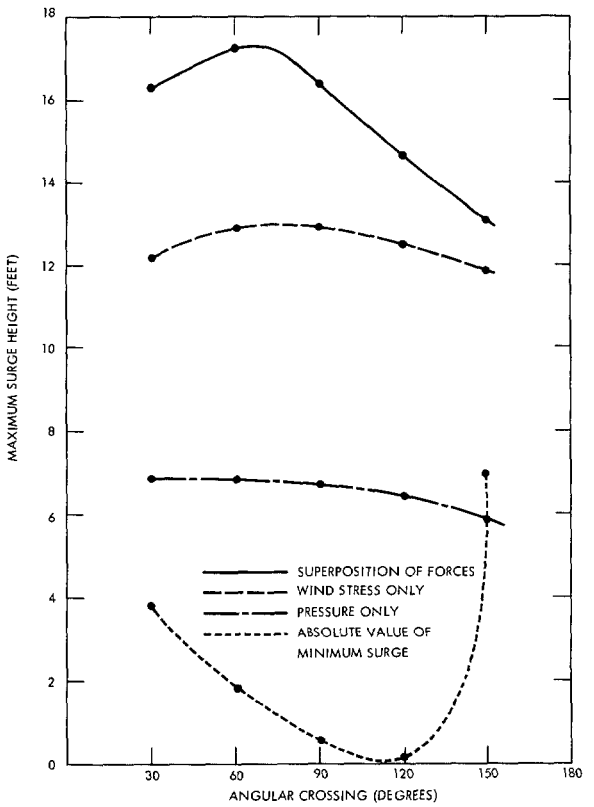

FIGURE 7.—The maximum coastal surge for the driving forces, and the minimum for superposition of forces, at different storm crossing angles to the coast; the storm speeds are all 30 m.p.h.

basins other than standard. These modifications, or corrections, are useful only if the actual or "on hand" storms and basins do not differ greatly from standard.

A typical pre-computed coastal surge profile is illustrated in figure 8. The observer is on the sea facing land. For a storm with landfall at point O, the positive surge GCBDF is considered sufficiently located by the five separate points when distance OA is prescribed. The maximum height of the surge is given by AB, the lowest surge value is given by IH; CD is the distance on the coast for surge values $\geq \frac{1}{2}$ AB (where CJ$\simeq$JD), EF is the distance for surge values $\geq \frac{1}{4}$ AB, and AG is the distance to zero surge on the coast. The profile at point H is occasionally too flat to readily define the distance AI.

A particular coastal surge profile is computed in the numerical model for fixed parameters of (1) latitude, (2) depth profile, (3) stationary storm maximum wind, (4) speed of storm motion, (5) direction of storm motion, and (6) radius of maximum wind. To see how the profile is influenced by these parameters, consider a standard storm in a standard basin and vary the last three parameters. Then contour the specialized heights and distance of figure 8 on polar charts, where rays are direction of storm motion (crossing angles) and radii are storm speeds. Let all storms be placed initially so that landfall occurs at the same time (5 hr. after start), except that storms which spend considerable time on the continental shelf are placed initially at least beyond the continental shelf.

Figures 9 a–b give the distance in miles from landfall to the maximum surge on the coast plotted against storm velocity. The contours are restricted to the wedge-shaped region outlined in broken lines and to storms traveling from sea to land. Notice that the contour distance is almost equivalent to the radius of maximum winds throughout the region except where edge wave phenomena occur. The contours of figure 9a were drawn from 25 separate calculations and of figure 9b from 21 different calculations.

Figures 10 a–b give contours of the maximum surge on the coast against storm velocity. It is interesting to note that higher surges occur for storms moving from relative northeast, all other things being equal. For operational purposes it possibly would be more appropriate to define a standard storm for fixed pressure instead of fixed maximum wind. Had this been done, figures 10 a–b would be nearly identical; this is so because the same pressure drop in storms gives a maximum wind that varies inversely as the radius of maximum wind (fig. 21) and hence opposes changes in surge formation. This bears out the conclusion of Conner, Kraft, and Harris [1], who found an empirical correlation between peak surges and pressure drop of storms.

Contours of the minimum surge on the coast as a function of storm velocity are shown in figure 11. Because of the general flatness of slope about this surge, the distance from it to the maximum surge was not always discernible. The minimum surge does not necessarily occur at time of maximum surge.

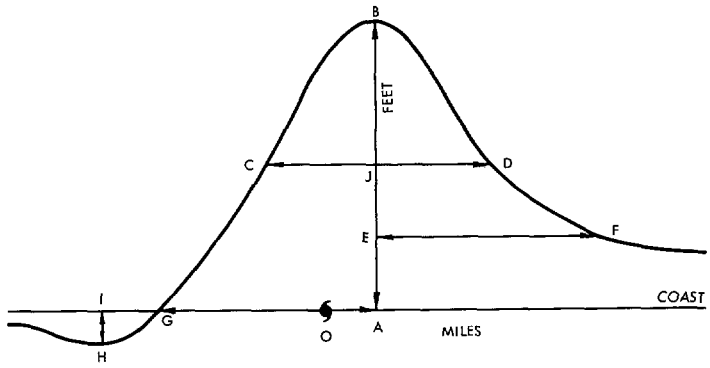

FIGURE 8.—A typical computed coastal surge profile. The observer is on sea facing land. The various heights and distances are for later reference.

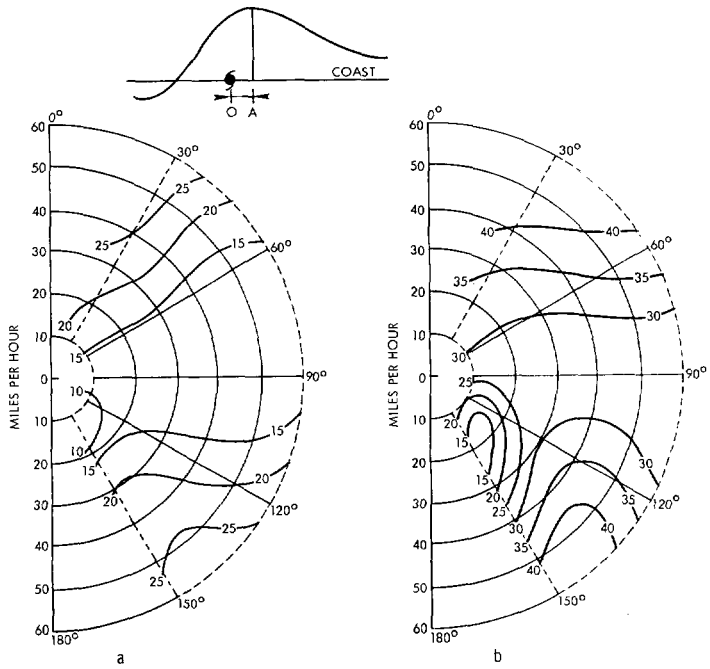

FIGURE 9.—Contours of distance in miles from landfall to maximum coastal surge. The arguments are speed and direction of uniform rectilinear storm velocity: concentric semicircles are storm speeds and rays are crossing angles of storm to coast. The small insert illustrates the storm surge profile of figure 8 and the distance contoured. (a) Radius of storm maximum wind, 15 mi. (b) Radius of storm maximum wind, 30 mi.

Figures 12 a–b give contours of distance on the coast, for surge values greater than or equal to $\frac{1}{2}$ the maximum surge, against storm velocity. The above distance is assumed in this study to have a symmetrical surge profile about the maximum surge, that is to say CJ$\approx$JD in figures 12 a–b; actually the computed distance JD was always slightly larger than CJ. The contours in the figures imply that the distance is roughly three times the radius of maximum winds.

Figures 13 a–b give distance contours on the right side of the coast from the maximum surge to the point on the coast having $\frac{1}{4}$ the maximum surge height.

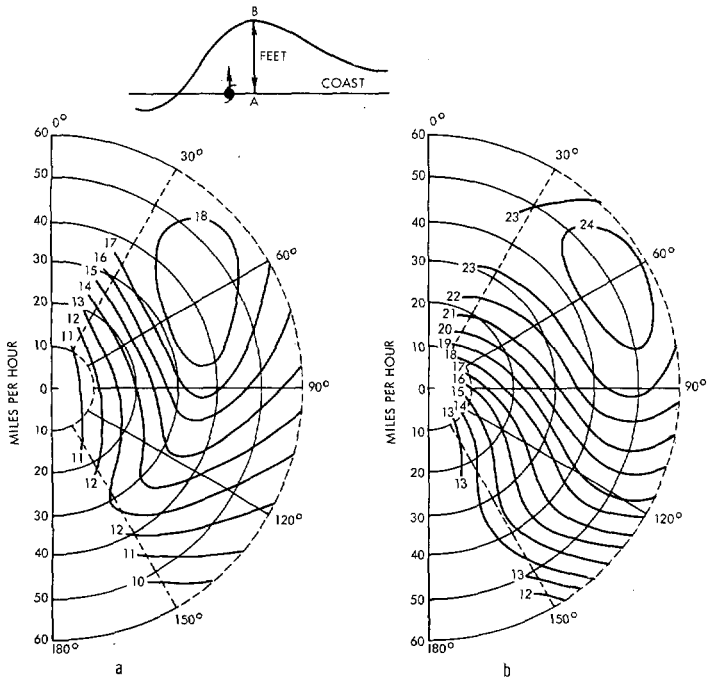

FIGURE 10.—Contours of maximum or peak coastal surge. The arguments are identical to figure 9.

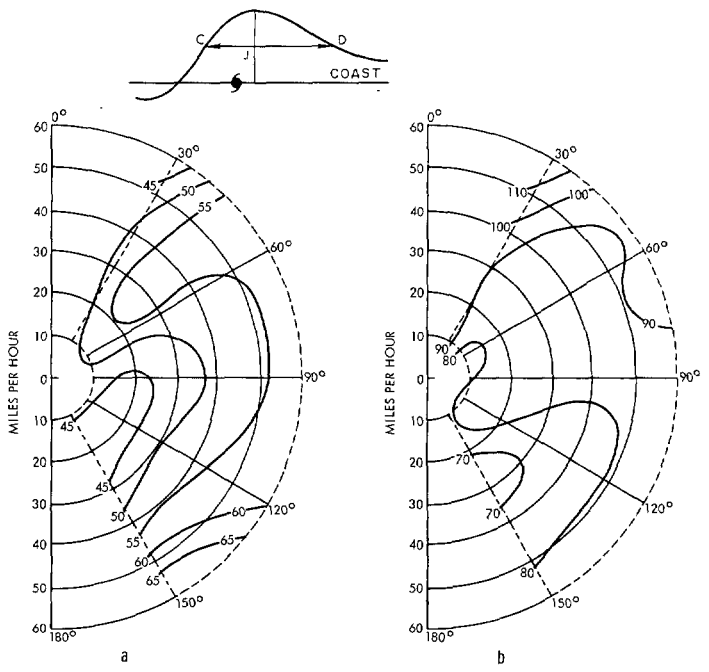

FIGURE 12.—Contours of distance on coast where surge is greater than ½ the maximum surge height. The arguments are identical to figure 9.

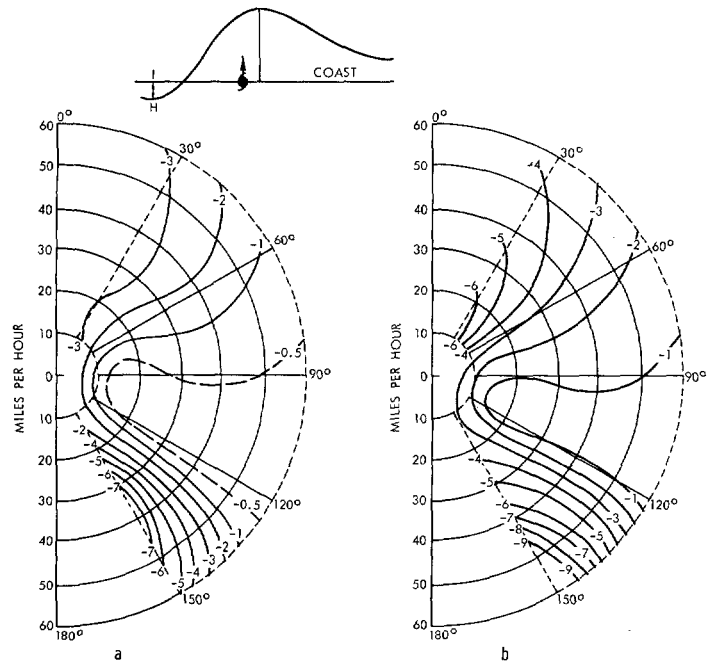

FIGURE 11.—Contours of minimum coastal surge. The arguments are identical to figure 9.

Figures 14 a–b give distance contours for the left side of the coast from the maximum surge to the point on the coast having zero surge. This distance, of all the distances discussed, is the least reliable in the numerical model.

Figures 15 a–b give the time, in minutes, of arrival of the maximum surge on the coast after landfall of the storm.

For slowly moving storms, especially those traveling at a small acute angle to the coast, the computed arrival time is sensitive to initial placement of the storm; consequently no attempt was made to contour arrival time in the figures for the slower moving storms.

In the construction of a practical forecasting system for storm surges, it is desirable to consider actual storms and basins that differ significantly from standard ones and to correct the coastal surge profile plotted from figures 10–14 without re-doing all previous computations for the new variable parameters of maximum wind, latitude, and depth profile. This will be done here, with the understanding that the "on hand" storms and basins do not differ greatly from the standard ones.

The driving forces in the numerical model were *so designed* that the surge is almost proportional to the wind parameter squared. The pressure drop of the model storm (Appendix 1) varies almost linearly with the wind parameter squared (fig. 21); this suggests that the surge from the pressure driving force is almost proportional to the wind speed squared.

The magnitude of the wind stress at any surface *point* of the basin varies approximately as the wind parameter squared. To show this, consider a storm moving at normal incidence to the coast. The ratio of the stress magnitude for any V_R to the stress magnitude for a standard storm, $V_R=100$ m.p.h. (see equation (A8) of Appendix 1), is

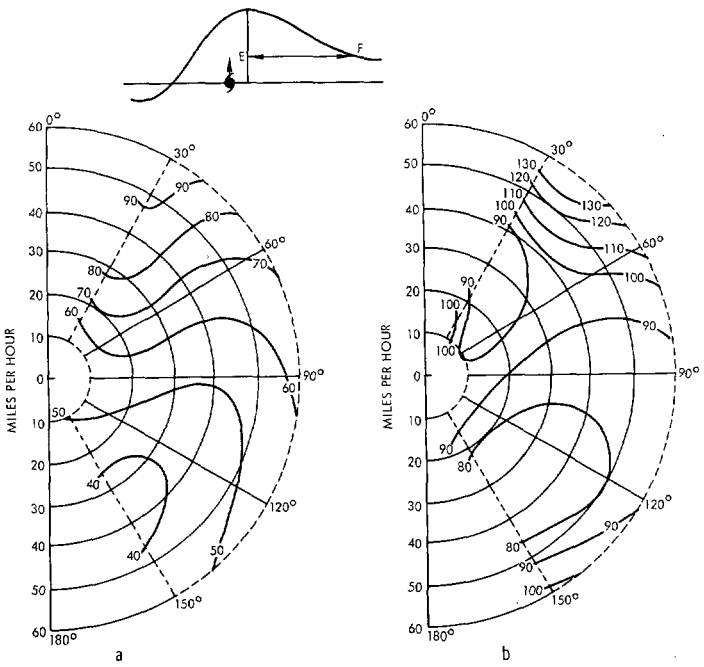

FIGURE 13.—Contours of distance on coast from maximum surge to ¼ the maximum surge height. The arguments are identical to figure 9.

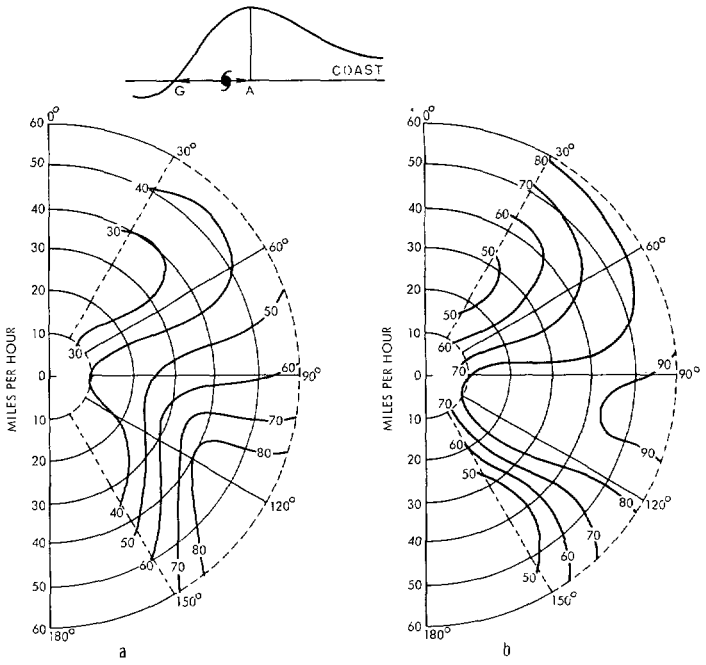

FIGURE 14.—Contours of distance on coast from maximum surge to zero surge. The arguments are identical to figure 9.

$$\left|\frac{(\tau)_{V_R}}{(\tau)_{100}}\right| = \frac{\left(\frac{U_s}{2V_R}\right)^2 - \frac{U_s}{V_R}\sin(\Theta+\phi_{V_R})+1}{\left(\frac{U_s}{2(100)}\right)^2 - \frac{U_s}{100}\sin(\Theta+\phi_{100})+1} \qquad (4)$$

The right side of (4) differs from unity only if the speed of the storm $U_s \neq 0$ and $V_R \neq 100$ m.p.h.; in the worst possible case ($U_s=60$ m.p.h.) the form remains within a few percentage points of unity providing the maximum wind does not greatly differ from standard. Separate computations with storms of differing maximum winds, velocities, etc. showed that the heights are almost proportional to the wind parameter squared and always agreed to within a few percentage points; there was no change in the dispersion of the surge on the coast.

Different values of the Coriolis parameter alter the two driving forces of the model storm to some extent and these in turn act to oppose changes in the surge due to change in latitude; consequently the numerically computed surge is almost conservative with respect to the Coriolis parameter for the model storms and basins of this study. In general the coastal surge increases only slightly with latitude. Test computations showed that the surge h varied almost linearly with latitude γ between latitudes 15° and 45° according to,

$$h=h_{30^\circ}\,[1.0+0.003\,(\gamma-30^\circ)]$$

We therefore define a latitude correction factor F_γ as

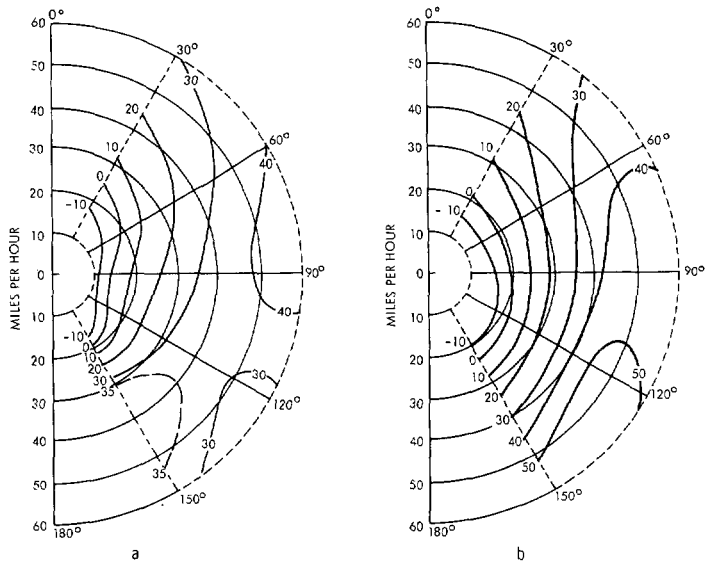

FIGURE 15.—The time of arrival (in minutes) of the maximum coastal surge after landfall of the storm. The arguments are identical to figure 9.

$$F_\gamma=1.0+0.003\,(\gamma-30^\circ) \qquad (5)$$

The total surge on the coast became slightly more dispersed with increasing latitude. The latitude correction factor for differing values of the remaining surge parameters would differ slightly from (5) but not in sense. The value

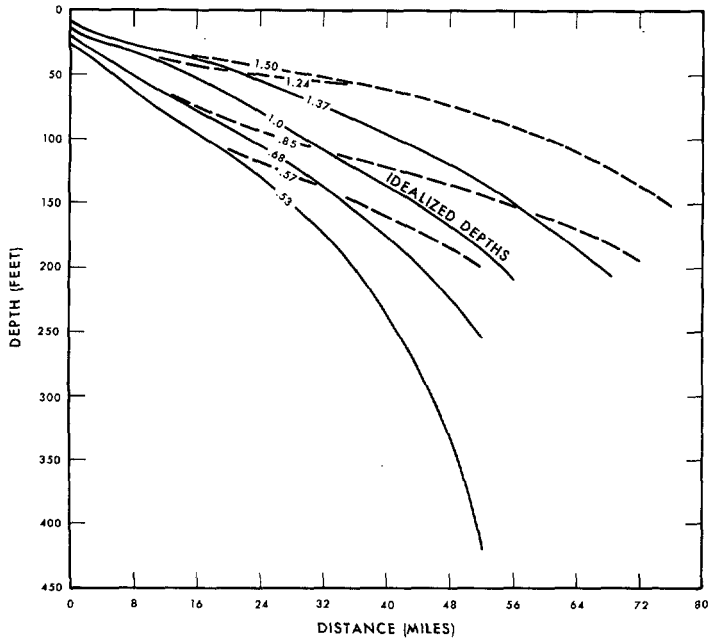

FIGURE 16.—Depth profiles simulating the range of depths off the Atlantic and Gulf coasts. The numbers on the profiles are corrections which can be applied to surges computed with the idealized depth profile.

of the factor does not differ greatly from unity within the range of latitude common to most storms and can be considered as an approximate correction for the entire positive surge height on the coast, providing the other fixed parameters do not differ radically from standard values.

Figure 16 illustrates some typical depth profiles off the Eastern and Gulf States of the United States. The numbers of the depth profiles are correction factors F_D to be applied to the computed surge profile when the depth is other than standard; they were determined by trial runs using standard storms. The contours of figures 10 a–b would follow a somewhat different pattern for depth profiles other than standard. This means that the correction factors of figure 16 are not invariant for different values of the other surge parameters, but the sense is always correct. Separate computations show that the depth correction factor does not differ to any great degree for the range of the various parameters in this study. Although the correction factors for *maximum surge* are significant, it is interesting to note that the various distances defined in figure 8 were altered very little. This is in contrast to varying the Coriolis parameter which caused heights and distances to change with approximately the same significance.

6. TEST OF THE MODEL

Two actual storms in the Gulf of Mexico will be considered to illustrate the mechanisms of storm surges. The region of the Gulf was chosen because storms there generally strike the coast at or near normal incidence, and the astronomical tide is small. Portions of the coast can be approximated by straight lines, except for the many bays and inlets. The various depth profiles off the coast vary roughly within the range of figure 16.

Hurricane Audrey struck the most shallow region of the Gulf coast on June 27, 1957 causing destructive storm surges (Harris [6]). This storm had a pressure drop of 57 mb., a radius of maximum winds of 22 mi., and maximum winds of 95 m.p.h. (cf. [2]). These values agree remarkably well with the nomogram of figure 21. The speed of the storm was about 16 m p.h. For the model storm, the values $R=22$ mi. and $V_R=95$ m.p.h. will be used; the latitude of landfall was almost 30°.

Figure 17 illustrates the coastal geography and depth patterns of the Gulf of Mexico in the vicinity of Audrey's landfall. The solid contour is the computed surge profile h_c derived from the standard profile h_s corrected for parameters different from standard, i.e.,

$$h_c=h_s\left(\frac{V_R}{100}\right)^2 F_\gamma F_D.$$

The actual depth profile normal to the shore varies along the coast; consequently F_D with values from figure 16, was applied at strategic points along the coast; correction for 2-dimensional depths in this manner is a good approximation even though the depth profile of the standard basin was constant.

The observed high crest values in figure 17 are from reporting tide gages. Just east of Cameron, high water marks between 10 and 14 ft. were measured by the U.S. Army Corps of Engineers (Harris [6]). The high crest values in Galveston Bay occurred before landfall and possibly can be explained as local effects in the bay; at time of landfall these gages were reading much smaller values.

Carla, an immense, slowly moving, and meandering storm finally struck the Texas coast, where waters in the Gulf are deepest, on September 11, 1961 at about 1600 EST. The latitude of landfall was about 28°. The observed surges from this storm are noteworthy not only for large amplitudes but also for the horizontal extent, or dispersion, and duration of the storm-induced tides (Harris [6]). The general coastline struck by this storm is fairly straight; the depths vary considerably in two dimensions.

Meteorological information on the storm is sparse. The pressure drop [2] was about 85 mb. A radius of maximum winds $R=25$ mi. was chosen; this gives $V_R=117$ m.p.h. from figure 21.[3] For somewhat larger or smaller R, the computed surge profile will not differ greatly; i.e., for the *same* pressure drop, the maximum wind varies inversely with R and changes in these two parameters

[2] The mean of several pressure drops about the storm, measured from the storm center to a point on an isobar where it begins to curve anticyclonically.

[3] For moderate changes in latitude (when latitude is other than 30°), the arguments do not change substantially except for the ingress or inflow angle. The storm surge is not unduly affected by changes of several degrees in the inflow angle.

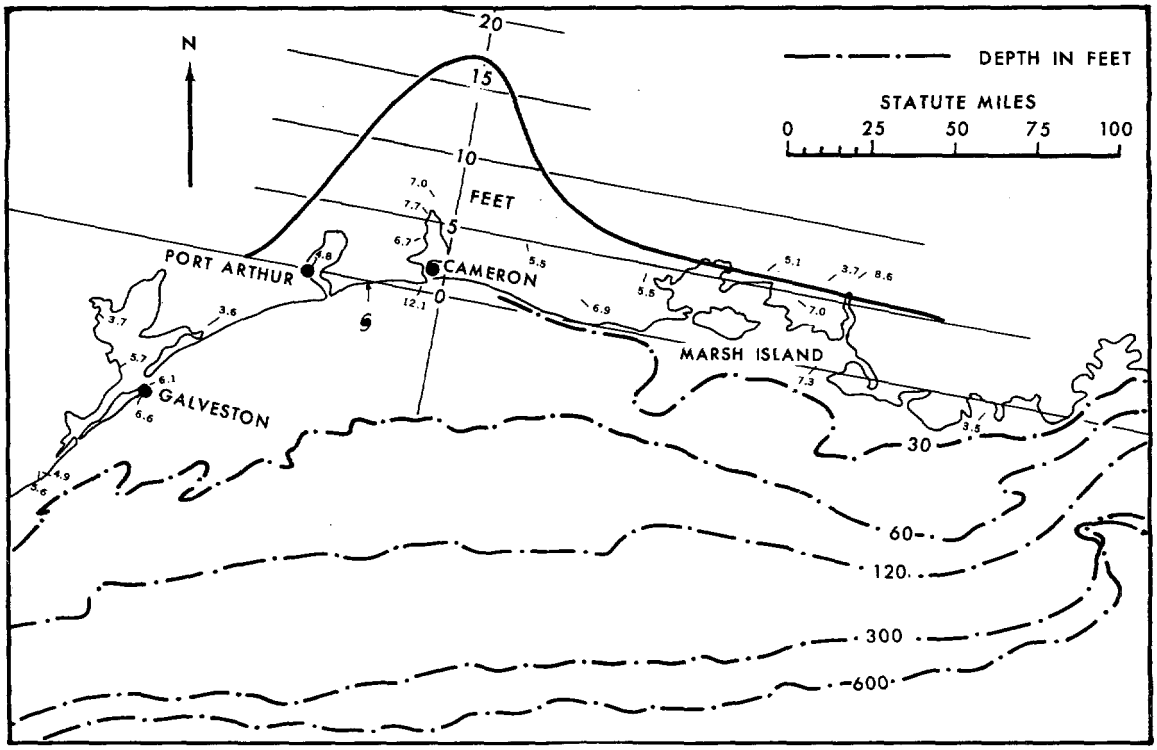

FIGURE 17.—Comparison of computed and observed coastal surges for hurricane Audrey. The solid line profile is the computed surge corrected for other than standard parameters of the storm and basin. The numbers distributed about the land and coastal areas are observed high water crests from recording tide gages (uncorrected for astronomical tide).

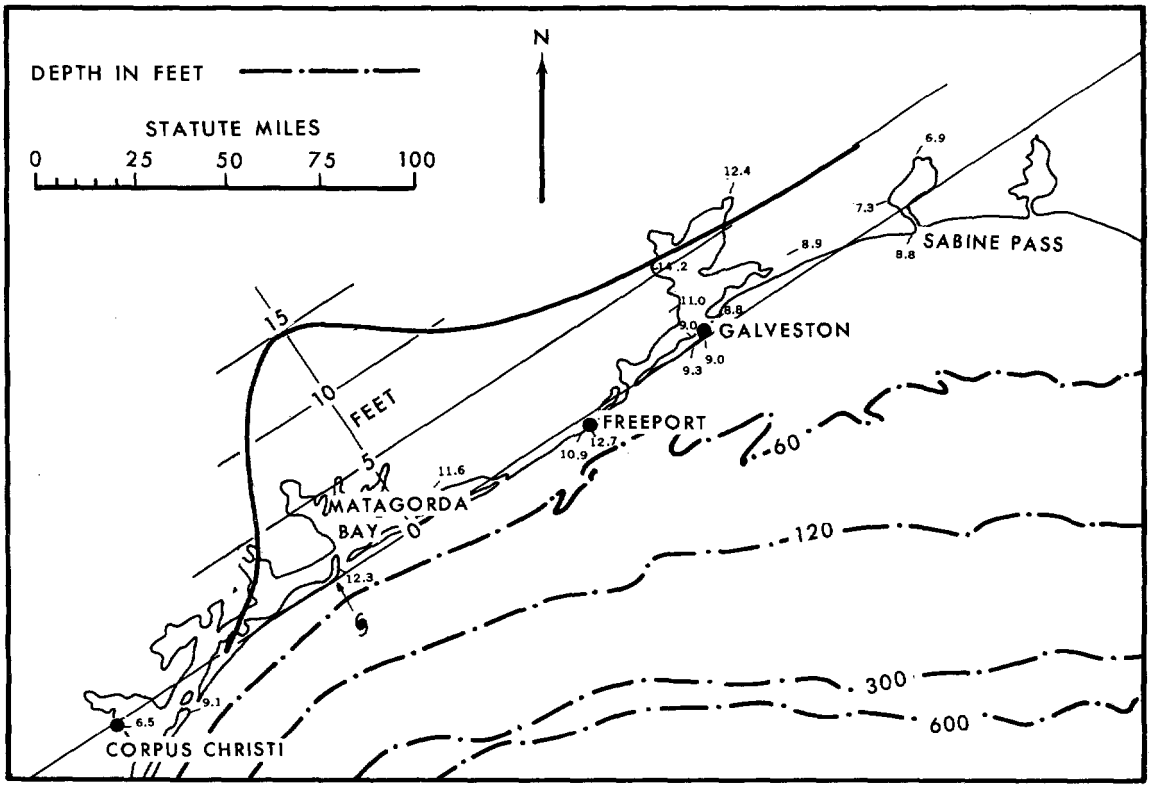

FIGURE 18.—Comparison of computed and observed coastal surges for hurricane Carla.

oppose each other in computed surge generation. The natural storm had an average speed of about 7 m.p.h.; however, near landfall the speed increased to about 10 m.p.h.

Figure 18 compares the computed coastal surge profile at time of maximum surge with observed high crest values from tide gages. The high crest in Corpus Christi Bay occurred about 6 hr. before landfall; at time of landfall the tides were much lower. Just north of Matagorda Bay, high water marks between 15 and 22 ft. were measured by the U.S. Army Corps of Engineers (Harris [6]).

Miyazaki [12] computed the surge of Carla using finite difference techniques that were very extensive and complete, with bottom stress, zig-zag boundaries, etc. He used driving forces at each time step that were interpolated polynomially from weather maps; his storm had maximum winds up to 100 m.p.h. and radius of maximum winds as large as 50 mi. The computed surges agreed very well with tide gages (corrected for astronomical tide) except for Port O'Connor (located near landfall of the storm); his highest surge values obtained were 9 ft. between landfall and Galveston. The peak surge of figure 18 did not appear in his computations.

In these tests of the model, it should be emphasized that inundation of the coastal areas is not considered; the boundary used in the computations is a rigid vertical wall. This means that for low-lying coastal areas prone to inundation, the model gives excessive surge heights because of reflection of the surge on the inserted vertical wall.

7. SUMMARY AND CONCLUSIONS

The numerical model without bottom friction is useful for computing short-duration transient coastal surges when generated by moderate or fast moving storms which do not travel parallel to the coast. For these storms test computations showed that the coastal surge is not sensitive to any bottom friction law, nor to initial placement of the storm, even when this is at large distances from landfall. The model storms were generally placed in the basin so that landfall occurred at least 5 hr. after start of computations, excepting slowly moving storms which were placed at least beyond the continental shelf.

The numerical model is not designed to handle storms having long duration on the continental shelf since the absence of a dissipating mechanism allows enormous transports to form eventually near the coast. For stationary or very slowly moving storms, the model generates shelf seiches of significant amplitudes, and the more so for model storms of large areal extent. For this reason only storms with speeds greater than 10 m.p.h. were considered in this study so as to allow initial placement at least beyond the continental shelf, and avoid the forming of enormous transports.

Computations made for storms traveling parallel or nearly parallel along the coast developed a type of resurgent edge wave that formed behind the storm track. The amplitude and wavelengths of these resurgences were dependent on the storm's speed, with very large amplitudes forming for fast moving storms in the absence of a dissipating mechanism. Therefore, storms crossing the coast with an angle greater than 30° only were considered as the elapsed time before landfall was then insufficient for large-amplitude resurgences to form.

Many features of the numerically computed storm surge bear out the empirical conclusions of Conner, Kraft, and Harris [1], and Harris [5]. In these studies a correlation was found between the peak surge and pressure drop of a storm, with no discernable correlation with the radius of maximum winds. The present study agrees with this providing the basin used is the same as that in the above studies and the storms travel with the same velocity. The changes in depth off the coast are found to be more significant in this report than in that by Harris [5].

By the methods of this study it is possible to construct a computed coastal storm surge profile when certain fixed parameters are specified. In spite of the idealizations in the numerical model (which consist of a straight-line coast, lack of bottom friction, simple wind stress law, and a storm model invariant in strength and traveling with uniform rectilinear velocity), this profile is of qualitative value in the understanding and forecasting of storm surges.

APPENDIX 1.—TROPICAL STORM MODELS

STATIONARY STORM

To develop a tropical storm model for application with the numerical storm surge model, which gives pressure drop, pressure gradient, and inflow angle, the method of wind trajectories at anemometer level was used. The equations of motion for this stationary storm model are given by Myers and Malkin [14] as,

$$\frac{1}{\rho_a}\frac{\partial p}{\partial r}=\frac{k_s v^2}{\sin\phi}-v\frac{\partial v}{\partial r} \tag{A1}$$

$$\frac{1}{\rho_a}\frac{\partial p}{\partial r}\cos\phi=fv+\frac{v^2}{r}\cos\phi-v^2\frac{\partial\phi}{\partial r}\sin\phi+k_n v^2. \tag{A2}$$

Consider a symmetric wind field about the storm's center with maximum wind V_R at distance R from the center. Let it be assumed that the wind speed v at distance r from the center is,

$$v=\frac{2V_R Rr}{R^2+r^2}. \tag{A3}$$

This wind function was an arbitrary choice to form a simple algebraic formulation of the wind speed. It is a highly idealized assumption and presupposes an average steady wind at any point from the storm's center.

If the pressure gradient is eliminated from (A1) and (A2), the resultant nonlinear ordinary differential equation of first order can be solved for ϕ by numerical techniques such as the Runge-Kutta method. It was deter-

mined from separate computations that changes in ϕ of several degrees for the entire storm do not affect the coastal storm surge significantly. Consequently in this study, the simple Newton-Raphson method was used to solve the equation with $d\phi/dr$ replaced, at first with zero, then with derivatives obtained from the preceding solutions. This iteration scheme was carried through only once since the next few iterations did not in general change significantly and for higher order iterations the solution became erratic as a result of round-off errors.[4]

At large distances from the storm's center, the wind, pressure gradient, and inflow angle have only a minor effect on the coastal storm surge. For this reason, and as a great convenience in computations, it was assumed that

$$\phi|_{r>100}=\phi|_{r=100}.$$

For the region $0\leq r<R$, it may be too drastic to assume constant friction coefficients in the core of the storm. For practical considerations, it was assumed that the inflow angle is zero at the center of the storm and was determined in this region by,

$$\phi=ar^3+br^2 \tag{A4}$$

where a and b are determined from known values of ϕ and $d\phi/dr$ at $r=R$.

Equation (A1) now readily determines the pressure gradient for a storm with circularly symmetric pressure profiles for $r\geq R$; however, for $r\leq R$ where the friction force is unknown, a different technique was used. Schloemer [19] gives a general relation for pressure as,

$$\frac{p-p_0}{p_\infty-p_0}=e^{-KR/r} \tag{A5}$$

where K is a fixed parameter for each individual storm; in this study $K=1$. One could determine a pressure gradient from (A5), but it would not be continuous with (A1) at $r=R$; therefore, continuity is forced by the following procedure. Equations (A1), (A3), and (A5) at $r=R$ give a pressure drop of,

$$(p_R-p_0)=\frac{\rho_a R k_s V_R^2}{K\sin\phi|_{r=R}}. \tag{A6}$$

If this is substituted in an equation of type (A4), then the derivative gives pressure gradient in the region $0\leq r\leq R$.

Computations with the present numerical model require static heights on a deep water open boundary. Since 30 mb. of pressure is almost 1 ft. of static height, only gross approximations for pressure drop are required. To determine the pressure drop of the model storm, a finite central difference form operating on the pressure gradient between $0\leq r\leq 100$ mi. and an integration of the pressure gradient for $r>100$ mi. were used.

Figure 19 represents the model stationary storm simulating the August 1949 storm over Lake Okeechobee. The values chosen for the computations were $V_R=82$ m.p.h., $R=22$ mi., and $f=0.238$/hr. The friction coefficients used were $k_s=0.022$/mi. and $k_n=0.02$/mi. given by Myers and Malkin [14]. The computed pressure drop is 62 mb.; the average observed pressure drop given by Schloemer [19] is 60 mb. The observed profiles given in figure 19 are averaged profile observations from scatter diagrams.

The friction coefficients for an enclosed lake are believed to be too high for storms in the open ocean. An investigation of hurricane Helene (Schauss [18]) gave open ocean friction coefficients of k_s, $k_n=0.009$, 0.007/n. mi. Figure 20 represents the model stationary storm simulating this storm. The observed profiles (right front quadrant) are averaged profiles from scatter diagrams of ship reports, winds determined from tracking small precipitation areas by radar, etc. The parameters chosen for computation were $V_R=106$ m.p.h., $R=26$ mi., and $f=0.278$/hr.

It was determined by separate computations that large changes in fixed values of the friction coefficients resulted in only small changes in the coastal storm surges, provided the inflow angle does not become large. Hence, a wide latitude of values for the friction coefficients is permissible in the storm surge numerical computations. The question arises how to choose these coefficients. Choosing the same fixed values, say those for hurricane Helene, for all storms would not be appropriate since large and erratic inflow angles result with storms having large V_R and small R.

It was decided to constrain the ingress angle to prevent any large angles in the storm region and also to prevent the occurrence of zero angle at any $r\geq R$. To this end, after several empirical trials, the following friction coefficients were designed,

$$k_s=10^{-2}\left[\frac{R}{.3V_R+60}\right]^{1/2};\quad k_n=10^{-2}\left[\frac{R}{.4V_R+80}\right]^{1/2}=0.867k_s$$

These forms maintain Schauss' values approximately for storms of Helene's size and have non-erratic inflow angles for all storms with R greater than 5 mi.

The friction coefficients above are not to be confused with the wind stress constant (equation (2) in section 2). To put the coefficients in the form of the wind stress constant, it would be necessary to integrate equations (A1), (A2) in the vertical through the depth of the inflow layer (Malkus and Riehl [11], Riehl [17]). The above forms are another way of saying that the inflow layer, and the inflow angle in the layer, differ for different storms.

Figure 21 is a nomogram, for latitude 30°, relating $(p_\infty-p_0)$, k_s, and $\phi|_{r=100\text{ miles}}$ against maximum winds (stationary storm) and the radius of maximum winds. The nomogram demonstrates some very useful properties of the storm model. For constant R, the pressure drop varies approximately as the square of V_R; since the wind stress also varies approximately with the square of V_R, then computations with the numerical model need be

[4] This method gave results that always differed by less than 2° from a Runge-Kutta method for storms used in this report.

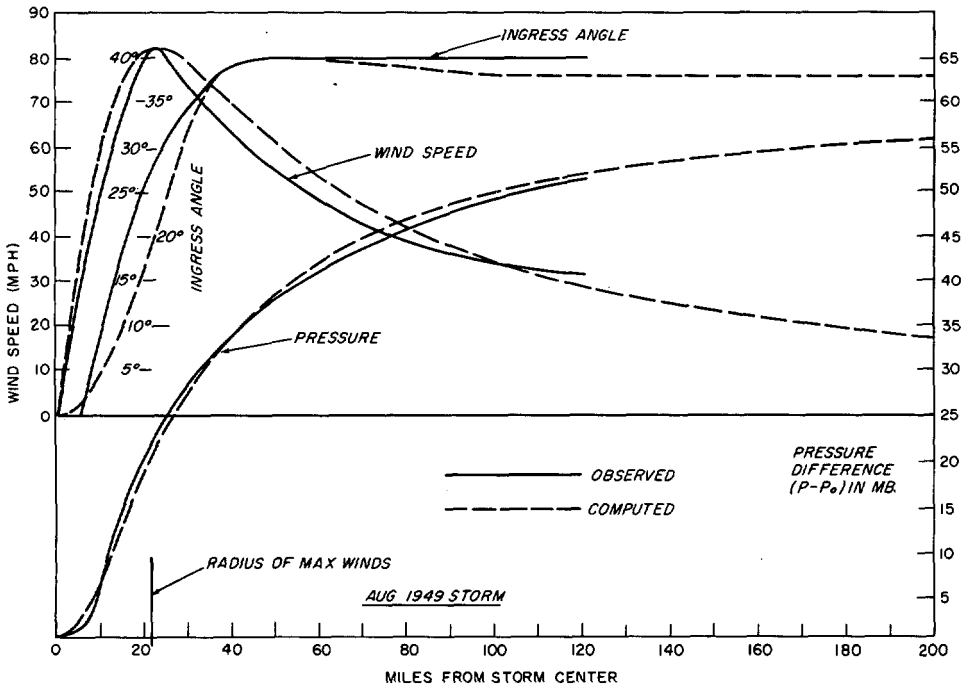

FIGURE 19.—Observed and computed wind, pressure, and inflow angle profiles for the August 1949 storm over Lake Okeechobee, Fla. The observed profiles are averaged from scatter diagrams (Myers and Malkin [14]).

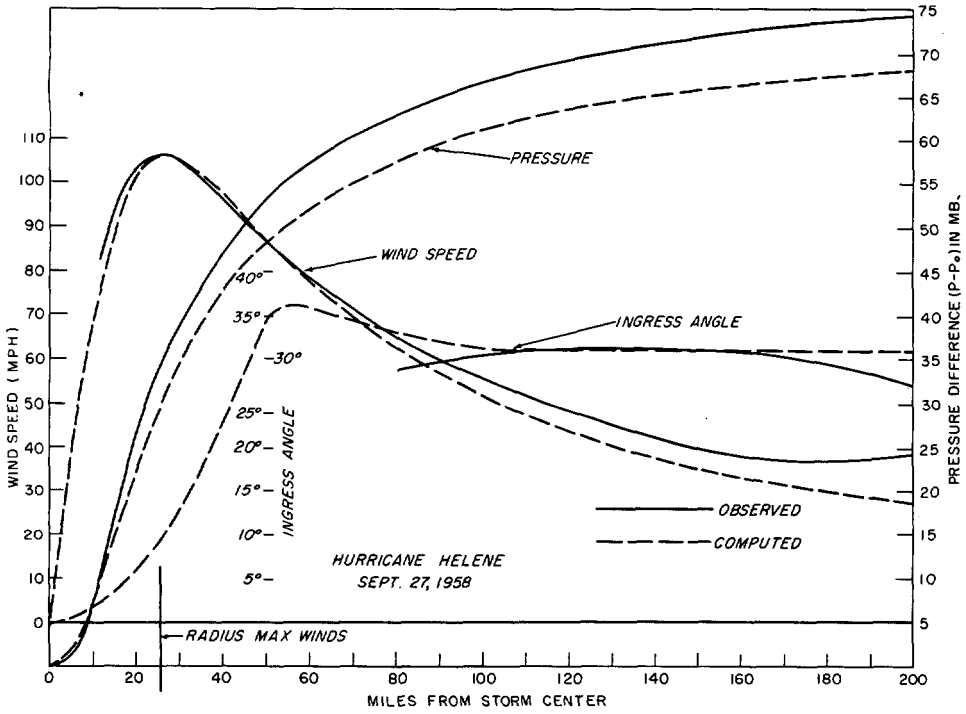

FIGURE 20.—Observed and computed wind, pressure, and inflow angle profiles for hurricane Helene, September 1958, right front quadrant. The observed profiles are averaged from scatter diagrams (Schauss [18]).

performed with only one standard V_R (100 m.p.h. in this report). For a constant pressure drop, V_R varies inversely with R; these two varying parameters oppose each other in storm surge generation, consequently *the surge is almost conservative for a constant pressure drop.* This is an extremely fortuitous property since only the pressure drop can be measured in nature with useful accuracy; one can then choose any reasonable R in the storm model to arrive at approximately the same peak surge on the coast.

MOVING STORM

A moving storm generally has an asymmetric wind field about the storm's center with stronger winds to the right (observer facing direction of storm motion). It was

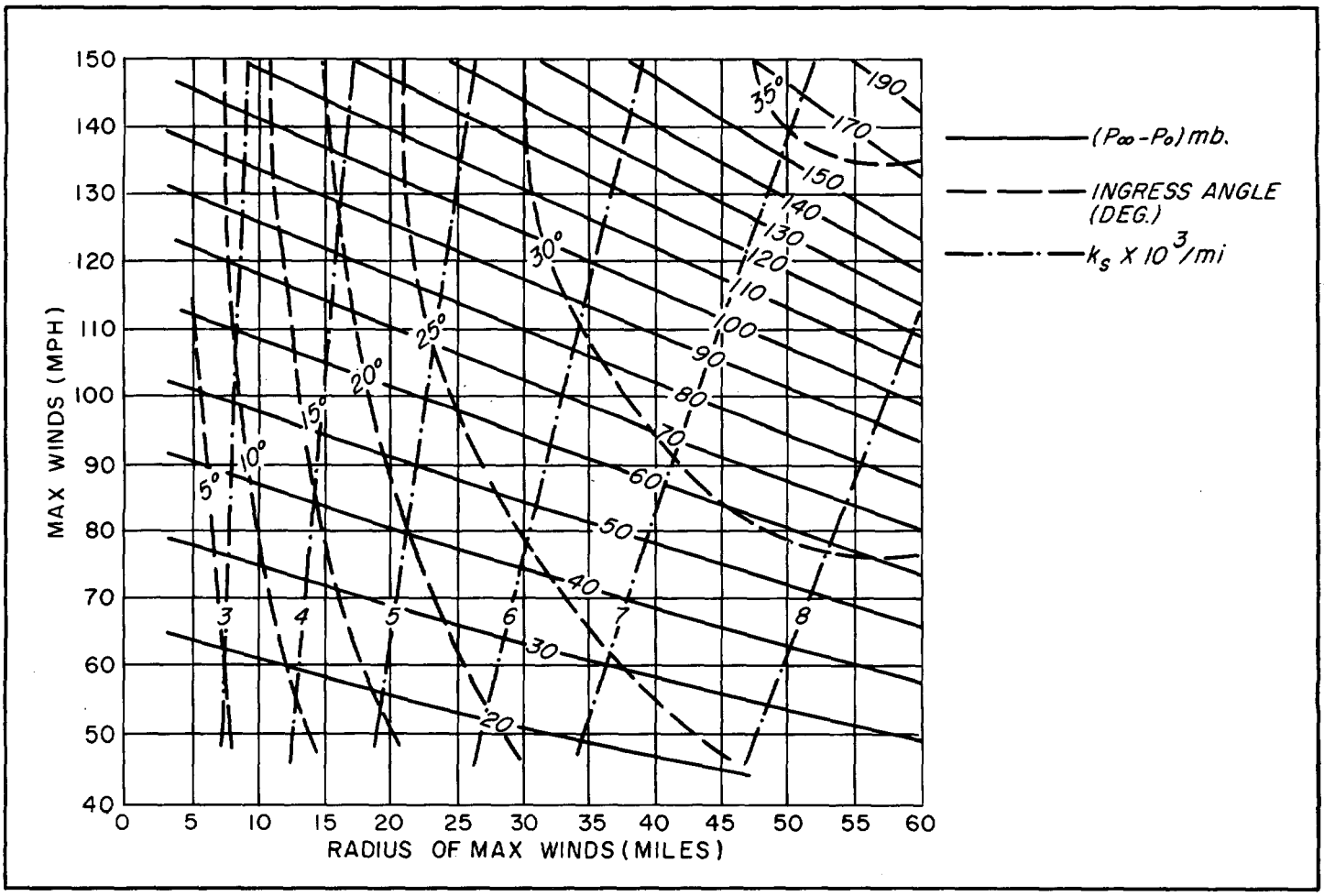

FIGURE 21.—A nomogram relating parameters of the model storm.

shown that an asymmetric wind field has some significance in generating the coastal storm surge (Jelesnianski [8]). In this study the stationary storm wind field vectors were altered by adding a vector derived from storm motion; the pressure field was not altered. Simplicity and convenience are the guiding themes for computing the effects of a moving storm, since the stationary storm wind field is considerably more effective than the pressure gradient or the added modification of an asymmetric wind field in governing the storm surge (Jelesnianski [8]).

In this study the vector $\mathbf{U}_{SM}$ added to the stationary storm wind vector for a gross correction for storm motion $\mathbf{U}_S$ is,

$$\mathbf{U}_{SM}=\frac{Rr}{R^2+r^2}\mathbf{U}_S. \tag{A7}$$

Only storms moving with uniform rectilinear motion are considered. Figure 22 illustrates the wind field for the August 1949 storm, if it were moving at 30 m.p.h., when computed by the methods of this study.

The wind stress used in the numerical storm surge model is,

$$\frac{\tau}{\rho}=\frac{k\rho_a}{\rho}|\mathbf{v}+\mathbf{U}_{SM}|(\mathbf{v}+\mathbf{U}_{SM})=\frac{k\rho_a}{\rho}\left[\frac{2RV_Rr}{R^2+r^2}\right]^2\sqrt{A^2+B^2}[A\mathbf{i}+B\mathbf{j}] \tag{A8}$$

where

$$A=\frac{U_S}{2V_R}\cos\Phi-\sin(\theta+\phi);\quad B=\frac{U_S}{2V_R}\sin\Phi+\cos(\theta+\phi)$$

In the numerical model, sin ϕ, cos ϕ, static heights, and pressure gradient at 1-mi. intervals from the storm center are stored in memory. The stored items could have an error in position as great as ½ mi.; the resulting storm surge error in the computations is miniscule.

APPENDIX 2.—SHELF SEICHES

A shelf seiche is a standing shelf oscillation. For a constant depth, nonrotating basin closed at both ends, the fundamental period of the standing wave or seiche is given by "Merian's formula,"

$$T=2L/\sqrt{gD}$$

where L is the length of the basin. If the basin is open at

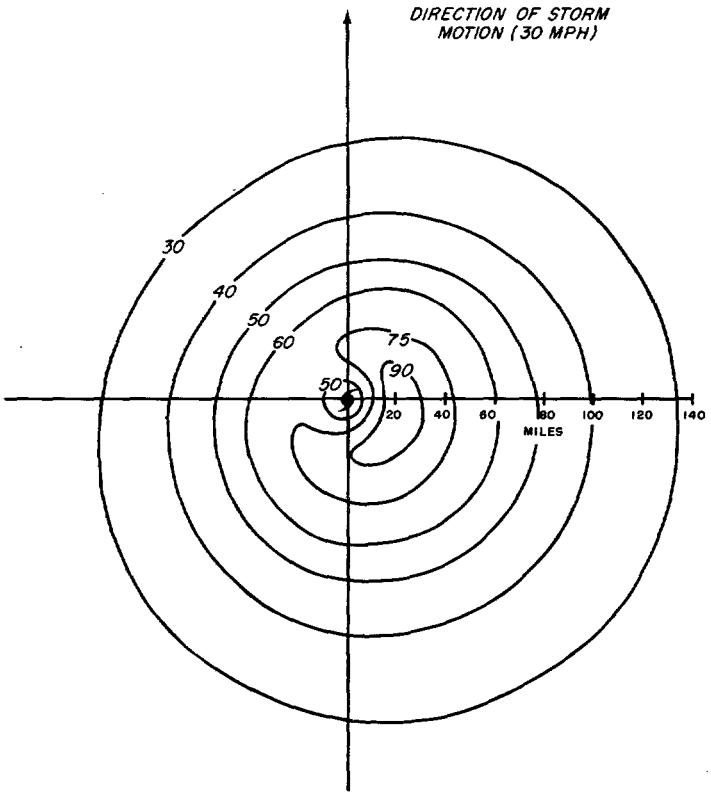

FIGURE 22.—The computed wind speed, in miles per hour, of a uniform rectilinear moving model storm.

one end (a shelf) and the first node of the standing wave is located at the open end then,

$$T=4L/\sqrt{gD}$$

For the idealized basin used in this study, the mean depth of the basin is about 115 ft. and $L=56$ mi. T in this case is about 5.4 hr. and in fair agreement with the numercially computed periods from figures 3 a–b (about 5.1 hr.). The static height on the deep water open boundary is invariant with time for a stationary storm, consequently node conditions prevail on the open boundary of the shelf.

Reid [16], arrived at a shelf seiche period for a linear sloping depth basin of,

$$J_0\left[2\sqrt{\frac{\left(\frac{2\pi}{T}\right)^2-f^2}{g\sin\beta}}L\right]=0$$

where J_0 is a Bessel function of the first kind and order zero. Lamb [10] arrives at the same function, with $f=0$, for a nonrotating sloping depth basin. If the first zero of this function is taken as a node at the open end of the basin, $f=0.73\times10^{-4}$, and $\sin\beta=200$ ft./56 mi., then T is about 5.3 hr.

REFERENCES

1. W. C. Conner, R. H. Kraft, and D. L. Harris, "Empirical Methods for Forecasting the Maximum Storm Tide Due to Hurricanes and Other Tropical Storms," *Monthly Weather Review*, vol. 85, No. 4, Apr. 1957, pp. 113–116.
2. H. E. Graham and G. N. Hudson, "Surface Winds Near the Center of Hurricanes (and other Cyclones)," NHRP Report Number 39, U.S. Weather Bureau, 1960, 200 pp. (see p. 123).
3. H. P. Greenspan, "The Generation of Edge Waves by Moving Pressure Distributions," *Journal of Fluid Mechanics*, vol. 1, No. 6, Dec. 1956, pp. 574–592.
4. W. Hansen, "Theorie zur Errechnung des Wasserstandes und der Strömungen in Randmeeren nebst Anwendungen," *Tellus*, vol. 8, No. 3, Aug. 1956, pp. 287–300.
5. D. L. Harris, "An Interim Hurricane Storm Surge Forecasting Guide," *NHRP* Report No. 32, U.S. Weather Bureau, 1959, 24 pp.
6. D. L. Harris, "Characteristics of the Hurricane Storm Surge," *Technical Paper* No. 48, U.S. Weather Bureau, 1963, 139 pp.
7. D. L. Harris and C. P. Jelesnianski, "Some Problems Involved in the Numerical Solutions of Tidal Hydraulic Equations," *Monthly Weather Review*, vol, 92, No. 9, Sept. 1964, pp. 409–422.
8. C. P. Jelesnianski, "A Numerical Computation of Storm Tides Induced by a Tropical Storm Impinging on a Continental Shelf," *Monthly Weather Review*, vol. 93, No. 6, June 1965, pp. 343–358.
9. K. Kajiura, "A Theoretical and Empirical Study of Storm Induced Water Level Anomalies," Texas A and M University, Dept. of Oceanography and Meteorology, A and M Project 202, Ref. 59-23F, Dec. 1959.
10. H. Lamb, *Hydrodynamics*, 6th ed., Cambridge University Press, 1932, 738 pp.
11. J. S. Malkus and H. Riehl, "On the Dynamics and Energy Transformations in Steady-State Hurricanes," *Tellus*, vol. 12, No. 1, Feb. 1960, pp. 1–20.
12. M. Miyazaki, "Numerical Computation of the Hurricane Carla Storm Surge (September 1961) near the Texas Louisiana Coast." Unpublished Manuscript.
13. W. H. Munk, F. Snodgrass, and G. Carrier, "Edge Waves on a Continental Shelf," *Science*, vol. 123, No. 3187, Jan. 1956, pp. 127–132.
14. V. A. Myers and W. Malkin, "Some Properties of Hurricane Wind Fields as Deduced from Trajectories," *NHRP* Report No. 49, U.S. Weather Bureau, 1961, 45 pp.
15. G. W. Platzman, "A Numerical Computation of the Surge of June 26, 1954 on Lake Michigan," *Geophysica*, vol. 6, No. 3/4, 1958, pp. 407–438.
16. R. O. Reid, "Effect of Coriolis Force on Edge Waves, (1) Investigation of the Normal Modes," *Journal of Marine Research*, vol. 16, No. 2, 1958, pp. 109–144.
17. H. Riehl, "Some Relations Between Wind and Thermal Structure of Steady State Hurricanes," *Journal of the Atmospheric Sciences*, vol. 20, No. 4, July 1963, pp. 276–287.
18. C. E. Schauss, "Reconstruction of the Surface Pressure and Wind Fields of Hurricane Helene," *NHRP* Report No. 59, U.S. Weather Bureau, 1962, 45 pp.
19. R. W. Schloemer, "Analysis and Synthesis of Hurricane Wind Patterns Over Lake Okeechobee, Florida," *Hydrometeorological Report* No. 31, U.S. Weather Bureau, Washington, D.C., 1954, 49 pp.
20. T. Ueno, "Non-Linear Numerical Studies on Tides and Surges in the Central Part of Seto Inland Sea," *Oceanographical Magazine*, vol. 16, Nos. 1–2, Dec. 1964, pp. 53–124.
21. F. Ursell, "Edge Waves on a Sloping Beach," *Proceedings of the Royal Society of London* (A), vol. 214, 1952.
22. B. W. Wilson, "Note on Surface Wind Stress over Water at Low and High Wind Speeds," *Journal of Geophysical Research*, vol. 65, No. 10, Oct. 1960, pp. 3377–3382.

[*Received October 15, 1965; revised April 8, 1966*]